Experimental study of active *LRC* circuits with $\mathcal{PT}$ symmetries

Joseph Schindler, Ang Li, Mei C. Zheng, F. M. Ellis, and Tsampikos Kottos

Department of Physics, Wesleyan University, Middletown, Connecticut 06459, USA

Mutually coupled modes of a pair of active *LRC* circuits, one with amplification and another with an equivalent amount of attenuation, provide an experimental realization of a wide class of systems where gain and loss mechanisms break the Hermiticity while preserving parity-time $\mathcal{PT}$ symmetry. For a value $\gamma_{\mathcal{PT}}$ of the gain and loss strength parameter the eigenfrequencies undergo a spontaneous phase transition from real to complex values, while the normal modes coalesce, acquiring a definite chirality. The consequences of the phase transition in the spatiotemporal energy evolution are also presented.

Parity ($\mathcal{P}$) and time-reversal ($\mathcal{T}$) symmetries, as well as their breaking, belong to the most basic notions in physics. Recently there has been much interest in systems which do not obey $\mathcal{P}$ and $\mathcal{T}$ symmetries separately but do exhibit a combined $\mathcal{PT}$ symmetry. Examples of such $\mathcal{PT}$-symmetric systems range from quantum field theories and mathematical physics [1–3] to atomic [4], solid state [5,6] and classical optics [7–15]. A $\mathcal{PT}$-symmetric system can be described by a phenomenological "Hamiltonian" $\mathcal{H}$. Such Hamiltonians may have a real energy spectrum, although in general are non-Hermitian. Furthermore, as some parameter γ that controls the degree of non-Hermiticity of $\mathcal{H}$ changes, a spontaneous $\mathcal{PT}$ symmetry breaking occurs. The transition point $\gamma = \gamma_{\mathcal{PT}}$ shows the characteristic behavior of an *exceptional point* (EP) where both eigenvalues and eigenvectors coalesce (for experimental studies of EP singularities of lossy systems, see Ref. [16]). For $\gamma > \gamma_{\mathcal{PT}}$, the eigenfunctions of $\mathcal{H}$ cease to be eigenfunctions of the $\mathcal{PT}$ operator, despite the fact that $\mathcal{H}$ and the $\mathcal{PT}$ operator commute [1]. This happens because the $\mathcal{PT}$ operator is antilinear, and thus the eigenstates of $\mathcal{H}$ may or may not be eigenstates of $\mathcal{PT}$. As a consequence, in the *broken $\mathcal{PT}$-symmetric phase*, the spectrum becomes partially or completely complex. The other limit where both $\mathcal{H}$ and $\mathcal{PT}$ share the same set of eigenvectors corresponds to the so-called *exact $\mathcal{PT}$-symmetric phase* in which the spectrum is real. This result led Bender and colleagues to propose an extension of quantum mechanics based on non-Hermitian but $\mathcal{PT}$-symmetric operators [1,2]. The class of non-Hermitian systems with a real spectrum has been extended by Mostafazadeh in order to include Hamiltonians with generalized $\mathcal{PT}$ (antilinear) symmetries [17].

While these ideas are still debatable, it was recently suggested that optics can provide a particularly fertile ground where $\mathcal{PT}$-related concepts can be realized [7] and experimentally investigated [8,9]. In this framework, $\mathcal{PT}$ symmetry demands that the complex refractive index obeys the condition $n(\vec{r}) = n^*(-\vec{r})$. $\mathcal{PT}$-synthetic materials can exhibit several intriguing features. These include among others, power oscillations and nonreciprocity of light propagation [7,9,11], absorption-enhanced transmission [8], and unidirectional invisibility [15]. In the nonlinear domain, such nonreciprocal effects can be used to realize a new generation of on-chip

isolators and circulators [10]. Other advances within the framework of $\mathcal{PT}$ optics include the study of Bloch oscillations [12], the realization of coherent perfect absorbers–lasers [14], and nonlinear switching structures [13]. Despite all these efforts and the consequent wealth of theoretical results associated with $\mathcal{PT}$ structures, to the best of our knowledge, only one experimental realization of a system with balanced gain and loss has been reported up to now [9]. These authors studied the light propagation in two coupled $\mathcal{PT}$-symmetric waveguides where the spontaneous $\mathcal{PT}$-symmetry-breaking "phase transition" [18] was confirmed. The analysis has relied on the *paraxial approximation* which, under appropriate conditions, maps the scalar wave equation to the Schrödinger equation, with the axial wave vector playing the role of energy and with a *fictitious* time, related to the propagation distance along the waveguide axis. However, to the best of our knowledge, an experimental investigation of $\mathcal{PT}$ systems in the *spatiotemporal* domain has, until now, remained unexplored.

The purpose of this Rapid Communication is to present a simple experimental setup which displays all the phenomena encountered in systems with generalized $\mathcal{PT}$ symmetries: a pair of coupled oscillators, one with gain and the other with loss. This "active" dimer is implemented with simple electronics, and allows a direct observation of a "phase transition" from a real to a complex eigenfrequency spectrum. At the $\mathcal{PT}$-breaking point, the normal modes coalesce and the relative phase differences of their components acquire a definite value that is dictated by the inductive coupling. We conclude with an investigation of the temporal behavior of the energy. The generic properties of pseudo-Hermitian dynamics are identified and traced back to the properties of the normal modes. Being free of theoretical approximations, and due to its relative simplicity in the experimental implementation, the *LRC* networks with $\mathcal{PT}$ symmetry can offer insights into the study of systems with generalized $\mathcal{PT}$ symmetries and a practical means for testing $\mathcal{PT}$ concepts.

The experimental circuit is shown schematically in Fig. 1. Each inductor is wound with 75 turns of no. 28 copper wire on 15-cm-diameter polyvinyl chloride (PVC) forms in a 6×6 mm loose bundle for an inductance of $L = 2.32$ mH.
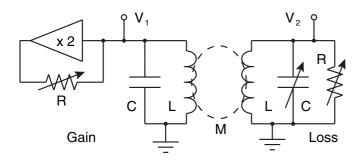
FIG. 1. Electronic implementation of a $\mathcal{PT}$-symmetric dimer. The negative resistance gain element is provided by feedback from a voltage-doubling buffer. The coils are inductively coupled, and V_1 and V_2 provide access to the system variables.

The coils are mounted coaxially with a bundle separation of 4.6 cm providing a mutual coupling of $\mu = M/L = 0.2$ used for this work. The $C = 10.7$ nF capacitances are silver mica, in parallel with the $\sim$320 pF coil bundle capacitance. The gain side is further trimmed with a GR722-M precision condenser. The resistors are carbon composite with the negative resistance gain provided by an LM356 operational amplifier (op-amp). The isolated natural frequency of each coil is $\omega_0 = 1/\sqrt{LC} = 2 \times 10^5$ s^{-1}.

The actual experimental circuit deviates from the ideal in the following ways: (1) A resistive component associated with coil wire dissipation is nulled out with an equivalent gain component applied to each coil; (2) a small trim is included in the gain buffer for balancing; and (3) additional LM356 voltage followers are used to buffer the measured voltages V_1 and V_2.

It is important to note that the linear nature of the system allows an exact balance of the $\mathcal{PT}$ symmetry only to the extent that component imbalance over a time scale necessary to perform a measurement is negligible. The real system modes ultimately either exponentially grow to the nonlinearity limit of the buffers, or shrink to zero. Experimental practice allows only for a marginal determination of gain and loss balance. The gain and loss parameter is set by choosing the loss-side resistance R (in the range 1–10 kΩ for this work) of Fig. 1, giving $\gamma = R^{-1}\sqrt{L/C}$, and matching the gain side R with the help of the gain trim. Our ability to balance the system parameters is estimated to be $\sim$0.1%.

Application of the first and second Kirchhoff's law, for the coupled circuits of Fig. 1, leads to the set of equations

$$I_n^C + I_n^R + I_n^L = 0, I_n^R = (-1)^n \gamma \omega_0 Q_n^C,$$
$$\omega_0^2 Q_1^C = \dot{I}_1^L + \mu \dot{I}_2^L, \omega_0^2 Q_2^C = \dot{I}_2^L + \mu \dot{I}_1^L, \quad (1)$$

where Q is the charge, I is the current, and $\dot{I} = dI/dt$. The superindices C, L, and R indicate that the quantity is associated with the capacitor, inductor, and resistor, while the subindices correspond to the amplified ($n = 1$) and lossy ($n = 2$) sides. Simple algebra allows us to rewrite Eqs. (1) for the charges $Q_n^C = CV_n$ in the form

$$\frac{d^2 Q_1^C}{d\tau^2} = -\frac{1}{1-\mu^2} Q_1^C + \frac{\mu}{1-\mu^2} Q_2^C + \gamma \frac{dQ_1^C}{d\tau},$$
$$\frac{d^2 Q_2^C}{d\tau^2} = \frac{\mu}{1-\mu^2} Q_1^C - \frac{1}{1-\mu^2} Q_2^C - \gamma \frac{dQ_2^C}{d\tau}, \quad (2)$$

where $\tau \equiv \omega_0 t$. Hence, all frequencies are measured in units of ω_0. Equations (2) are invariant under a combined $\mathcal{P}$ (i.e., $n = 1 \leftrightarrow n = 2$) and $\mathcal{T}$ (i.e., $t \rightarrow -t$) transformation.

In fact, Eqs. (2) can be recast in a "rate equation" form by making use of a Liouvillian formalism

$$\frac{d\Psi}{d\tau} = \mathcal{L}\Psi, \quad \mathcal{L} = \begin{pmatrix} 0 & 0 & 1 & 0 \\ 0 & 0 & 0 & 1 \\ -\frac{1}{1-\mu^2} & \frac{\mu}{1-\mu^2} & \gamma & 0 \\ \frac{\mu}{1-\mu^2} & -\frac{1}{1-\mu^2} & 0 & -\gamma \end{pmatrix}, \quad (3)$$

where $\Psi \equiv (Q_1^C, Q_2^C, \dot{Q}_1^C, \dot{Q}_2^C)^T$. It can be shown [19] that there exists a similarity transformation mapping the matrix $i\mathcal{L}$ to a $\mathcal{PT}$-symmetric Hamiltonian H. This formulation opens alternate directions for applications [19] of generalized $\mathcal{PT}$ mechanics [17].

We are interested in the evolution of eigenfrequencies, and normal modes of our system as the gain and loss parameter γ increases. The *exact* phase will be associated with the γ regime for which the eigenfrequencies ω_l are real, while the broken phase corresponds to the regime where one or all the eigenfrequencies ω_l become complex.

The eigenfrequencies ω_l can be found either by a direct diagonalization of the matrix $\mathcal{L}$, or by solving the secular equation resulting from Eq. (2) after the substitution $Q_n^C = A_n \exp(i\omega\tau)$. We get

$$\omega_{1,4} = \pm \sqrt{-\frac{2 + \gamma^2(\mu^2 - 1) + \sqrt{4(\mu^2 - 1) + [2 + \gamma^2(\mu^2 - 1)]^2}}{2(\mu^2 - 1)}}$$

$$\omega_{2,3} = \pm \sqrt{-\frac{2 + \gamma^2(\mu^2 - 1) - \sqrt{4(\mu^2 - 1) + [2 + \gamma^2(\mu^2 - 1)]^2}}{2(\mu^2 - 1)}}$$

$$(4)$$

For $\gamma = 0$, we have two frequency pairs $\omega_{1,4} = \pm\sqrt{1/(1-\mu)}$ and $\omega_{2,3} = \pm\sqrt{1/(\mu+1)}$. These modes are associated with the pair of double-degenerate frequencies $\omega = \pm 1$ related to a single isolated circuit ($\mu = 0$). At $\gamma = \gamma_{\mathcal{PT}}$, these eigenmodes

undergo a level crossing and branch out into the complex plane, with

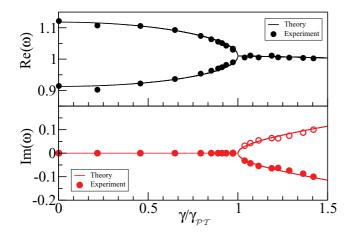$$\gamma_{\mathcal{PT}} = 1/\sqrt{1-\mu} - 1/\sqrt{1+\mu}. \quad (5)$$

FIG. 2. (Color online) Parametric evolution of the experimentally measured eigenfrequencies vs the normalized gain and loss parameter $\gamma/\gamma_{\mathcal{PT}}$. A comparison with the theoretical results of Eq. (4) indicate an excellent agreement. In all cases, we show only the $\mathrm{Re}(\omega_l) > 0$ eigenfrequencies. The open circles in the lower panel are reflections of the experimental data (lower curve) with respect to the $\mathrm{Im}(\omega) = 0$ axis.

Near $\gamma_{\mathcal{PT}}$ the eigenvalues display the characteristic behavior $|\omega| \propto \pm\sqrt{\gamma^2 - \gamma_{\mathcal{PT}}^2}$. This square-root singularity is a generic feature of the $\mathcal{PT}$-symmetry breaking. A second crossing between the pairs of degenerate frequencies (and another branching) occurs for a larger value $\gamma_2 = \sqrt{1/(1-\mu)} + \sqrt{1/(1+\mu)}$. For $\gamma > \gamma_2$ all frequencies are imaginary. Since this large γ regime is physically impractical, we will confine ourselves to values of $\gamma < \gamma_2$.

In Fig. 2 we report our measurements for the frequencies and compare them with Eq. (4). Our setup allows a detailed analysis for gain and loss parameters γ on either side of the $\mathcal{PT}$-phase transition point. In the exact phase $\gamma < \gamma_{\mathcal{PT}}$ the eigenfrequencies are obtained by trimming both the gain and capacitance balance until both modes become simultaneously marginal. The imaginary part of the frequency is then zero by construction. Individual modes are then measured by slightly unbalancing the trim for marginal oscillation of that mode. The amplitude grows to the nonlinearity-limited amplitude, and the voltage wave forms in both coils are captured and analyzed for frequency and relative phase. The values obtained are checked to assure that they are independent of the small imbalances applied, typically less than 0.3%.

In the broken phase $\gamma > \gamma_{\mathcal{PT}}$ marginal oscillation is not possible: The gain and capacitance trim are kept fixed at the values obtained in the exact phase near $\gamma_{\mathcal{PT}}$. The resistances R (and $-R$) are inserted, and the gain side coil is temporarily short circuited to prevent oscillation. The short is then removed, and the subsequent oscillatory growth triggers the wave-form capture. The wave forms in both coils are analyzed, including an exponential growth factor. With this method, only the exponentially growing mode with $\mathrm{Im}(\omega) < 0$ is observed.

Very close to $\gamma \sim \gamma_{\mathcal{PT}}$ attempts to trim the dimer to the marginal configuration result in either $V = 0$ (too small gain), or a chaotic interplay of the two modes with the op-amp nonlinearity if the gain is larger. This behavior serves as an indication that $\gamma_{\mathcal{PT}}$ has been exceeded.
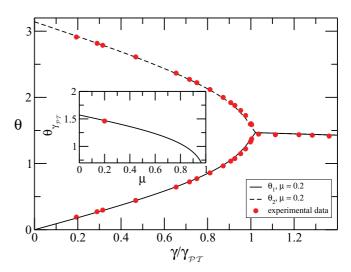

FIG. 3. (Color online) Parametric evolution of the phase difference $\theta_l = \phi_2^{(l)} - \phi_1^{(l)}$. The experimental measurements for $\mu = 0.2$ are shown in filled circles and match well the theoretical predictions (lines). The theoretical $\theta_{\mathcal{PT}}(\mu)$ is shown in the inset.

Another manifestation of $\mathcal{PT}$ symmetry is the relative phase difference $\theta_l = \phi_2^{(l)} - \phi_1^{(l)}$ between the two components $(Q_1^{(l)}, Q_2^{(l)})^T = (|Q_1^{(l)}|\exp(i\phi_1^{(l)}), |Q_2^{(l)}|\exp(i\phi_2^{(l)}))^T$ of the lth eigenmode. Experimentally, $Q_n^{(l)}(t) = CV_n(t)$ when mode (l) is marginally oscillated. The $\mathcal{PT}$ symmetry imposes the condition that the magnitude of the two components of the charge vector are equal to one another in the exact phase. For $\gamma = 0$, the phases corresponding to the symmetric and antisymmetric combination are $\theta_1 = 0$ and $\theta_2 = \pi$, respectively. When γ is subsequently increased and the system is below the $\mathcal{PT}$ threshold, the eigenstates are not orthogonal and their phases can be anywhere (depending on $\gamma/\gamma_{\mathcal{PT}}$) in the interval $[0, \pi]$. An example of the parametric evolution of phases is reported in Fig. 3, where the experimental measurements are plotted together with the theoretical results. The value of the phase difference $\theta_{\mathcal{PT}}(\mu) \equiv \theta(\mu, \gamma_{\mathcal{PT}})$ at $\gamma = \gamma_{\mathcal{PT}}$ can be calculated analytically and it is given by the expression

$$\theta_{\mathcal{PT}}(\mu) = \arccos\left(\sqrt{1 - \sqrt{1-\mu^2}}\Big/\sqrt{1 + \sqrt{1+\mu^2}}\right). \quad (6)$$

We note that in the limit of $\mu \to 0$ we get $\theta_{\mathcal{PT}} = \pi/2$, corresponding to a "circular" polarization of the eigenmode. The opposite limit of $\mu \to 1$ is associated with a broken time-reversal symmetry [20] and is reflected in the strong asymmetry of the $\mathcal{L}$ matrix for large μ values.

The signatures of $\mathcal{PT}$ symmetry and the transition from the exact phase to the broken phase are reflected in the temporal behavior of our system. We have traced these universal features by studying the time dependence of the total capacitance energy

$$E_C^{\mathrm{tot}}(\tau) = \frac{1}{2C}(Q_1(\tau), Q_2(\tau))(Q_1(\tau), Q_2(\tau))^T. \quad (7)$$

The initial condition used in the experiment corresponds to the case $I_1^L = I_{\mathrm{init}}$, with all other dynamical variables zero. With the appropriate R inserted and the dimer trim either marginal (exact phase) or fixed (broken phase), the initial current is injected into the gain side by connecting the V_1 node of Fig. 1
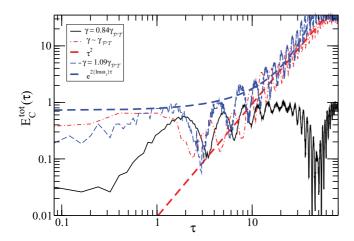
FIG. 4. (Color online) Experimentally measured temporal dynamics of the capacitance energy $E_C^{\text{tot}}(\tau)$ of the total system for various γ values. As $\gamma \to \gamma_{\mathcal{PT}}$, the τ^2 behavior signaling the spontaneous $\mathcal{PT}$-symmetry breaking is observed.

to a voltage source through a resistor. Oscillation in the broken phase is suppressed by the additional ac dissipation. Again, wave-form capture is triggered by removing the injection resistor.

Even though the frequencies are real for $\gamma < \gamma_{\mathcal{PT}}$, the total energy of the system E^{tot} is not conserved. Instead, we expect power oscillations which are due to the unfolding of the nonorthogonal eigenmodes [1,7,9,11]. This is evident in the temporal behavior of $E_C^{\text{tot}}(\tau)$ (see Fig. 4). For $\gamma > \gamma_{\mathcal{PT}}$ the dynamics is unstable and $E_C^{\text{tot}}(\tau)$ grows exponentially, with a rate given by the maximum imaginary eigenvalue $\max\{\text{Im}(\omega_l)\}$ (see Fig. 4).

The most interesting behavior appears at the spontaneous $\mathcal{PT}$-symmetry-breaking point $\gamma = \gamma_{\mathcal{PT}}$. At this point the

matrix $\mathcal{L}$ has a defective eigenvalue. In this case, the evolution $U = \exp(\mathcal{L}\tau)$ can be calculated from the Jordan decomposition of $\mathcal{L}$ as $\mathcal{J} = S\mathcal{L}S^{-1}$. Having in mind the form of the exponential of a Jordan matrix, it follows immediately that linear growing terms appear in the evolution of the charge vector $(Q_1(\tau), Q_2(\tau))^T$ [21]. This results in a quadratic increase of the capacitance energy, i.e., $E_C^{\text{tot}}(\tau) \sim \tau^2$. Although all systems typically become very sensitive to parameters near a critical point, we are able to control the circuit elements sufficiently well to observe the approach to the predicted τ^2 behavior of the energy. The time range is limited by the dynamic range of our circuit linearity.

In conclusion, we demonstrated that a pair of coupled, active *LRC* circuits, one with amplification and the other with equivalent attenuation, exhibits $\mathcal{PT}$ symmetry. This minimal example, which is experimentally simple and mathematically transparent, displays all the universal phenomena encountered in systems with generalized $\mathcal{PT}$ symmetries. At the same time, the accessibility of experimental quantities of interest enable us to perform accurate investigations and comparisons with theoretical predictions. We envision that their use will allow experimental studies in the spatiotemporal domain of more complicated structures, and shed light on scattering phenomena [22] recently proposed in the realm of generalized $\mathcal{PT}$ symmetries [14,15,23–25]. From integrated tuning of antenna arrays to real-time control of exotic metamaterials, the wealth of problems which have their counterparts in $\mathcal{PT}$ electronic circuits, and the lessons they can teach, are far from being exhausted.

[1] C. M. Bender and S. Boettcher, Phys. Rev. Lett. **80**, 5243 (1998); C. M. Bender, Rep. Prog. Phys. **70**, 947 (2007).

[2] C. M. Bender, S. Boettcher, and P. N. Meisinger, J. Math. Phys. **40**, 2201 (1999).

[3] C. M. Bender, D. C. Brody, and H. F. Jones, Phys. Rev. Lett. **89**, 270401 (2002); C. M. Bender, D. C. Brody, H. F. Jones, and B. K. Meister, *ibid*. **98**, 040403 (2007).

[4] E. M. Graefe, H. J. Korsch, and A. E. Niederle, Phys. Rev. Lett. **101**, 150408 (2008); M. K. Oberthaler, R. Abfalterer, S. Bernet, J. Schmiedmayer, and A. Zeilinger, *ibid*. **77**, 4980 (1996).

[5] O. Bendix, R. Fleischmann, T. Kottos, and B. Shapiro, Phys. Rev. Lett. **103**, 030402 (2009); C. T. West, T. Kottos, and T. Prosen, *ibid*. **104**, 054102 (2010).

[6] Y. N. Joglekar, D. Scott, M. Babbey, and A. Saxena, Phys. Rev. A **82**, 030103(R) (2010).

[7] K. G. Makris, R. El-Ganainy, D. N. Christodoulides, and Z. H. Musslimani, Phys. Rev. Lett. **100**, 103904 (2008); Z. H. Musslimani, K. G. Makris, R. El-Ganainy, and D. N. Christodoulides, *ibid*. **100**, 030402 (2008).

[8] A. Guo *et al*., Phys. Rev. Lett. **103**, 093902 (2009).

[9] C. E. Ruter *et al*., Nat. Phys. **6**, 192 (2010).

[10] H. Ramezani, T. Kottos, R. El-Ganainy, and D. N. Christodoulides, Phys. Rev. A **82**, 043803 (2010).

[11] M. C. Zheng, D. N. Christodoulides, R. Fleischmann, and T. Kottos, Phys. Rev. A **82**, 010103 (2010).

[12] S. Longhi, Phys. Rev. Lett. **103**, 123601 (2009).

[13] A. A. Sukhorukov, Z. Xu, and Y. S. Kivshar, Phys. Rev. A **82**, 043818 (2010).

[14] S. Longhi, Phys. Rev. A **82**, 031801 (2010); Y. D. Chong, L. Ge, and A. D. Stone, Phys. Rev. Lett. **106**, 093902 (2011)

[15] Z. Lin *et al*., Phys. Rev. Lett. **106**, 213901 (2011).

[16] C. Dembowski, H. D. Graf, H. L. Harney, A. Heine, W. D. Heiss, H. Rehfeld, and A. Richter, Phys. Rev. Lett. **86**, 787 (2001); T. Stehmann, W. D. Heiss, and F. G. Scholtz, J. Phys. A **37**, 7813 (2004).

[17] A. Mostafazadeh, J. Math. Phys. **44**, 974 (2003).

[18] We use the term "phase transition" not in the standard thermodynamic sense but rather in the frame of $\mathcal{PT}$ literature (see, for example, Ref. [1]).

[19] J. Schindler *et al.* (unpublished).

[20] B. Dietz *et al.*, Phys. Rev. Lett. **106**, 150403 (2011).

[21] S. K. Godunov, *Ordinary Differential Equations with Constant Coefficients* (American Mathematical Society, Providence, RI, 1997).

[22] J. Schindler *et al.* (unpublished).

[23] F. Cannata, J.-P. Dedonder, and A. Ventura, Ann. Phys. **322**, 397 (2007).

[24] A. Mostafazadeh, Phys. Rev. Lett. **102**, 220402 (2009).

[25] H. Schomerus, Phys. Rev. Lett. **104**, 233601 (2010).